Journal of Power Sources 194 (2009) 1029–1035

Contents lists available at ScienceDirect

Journal of Power Sources

journal homepage: www.elsevier.com/locate/jpowsour

Physical and electrochemical properties of $LiFePO_4$ nanoparticles synthesized by a combination of spray pyrolysis with wet ball-milling

Muxina Konarova, Izumi Taniguchi*

Department of Chemical Engineering, Graduate School of Science and Engineering, Tokyo Institute of Technology 2-12-1 Ookayama, Meguro-ku, Tokyo 152-8552, Japan

ARTICLE INFO

Article history:
Received 5 March 2009
Received in revised form 1 June 2009
Accepted 15 June 2009
Available online 24 June 2009

Keywords:
$LiFePO_4$
Nanoparticles
Spray pyrolysis
Wet ball-milling
Lithium-ion batteries
Cathode

ABSTRACT

A novel preparation technique was developed to synthesize $LiFePO_4$ nanoparticles through a combination of spray pyrolysis (SP) with wet ball-milling (WBM). Using this technique, the preparation of $LiFePO_4$ nanoparticles was investigated for a wide range of process parameters such as ball-milling time and sintering temperature. The effect of process parameters on the physical and electrochemical properties of $LiFePO_4$ was then discussed through analysis using by X-ray diffraction (XRD), field emission scanning electron microscopy (FE-SEM), transmission electron microscopy (TEM), the Brunauer–Emmet–Teller (BET) method, Raman spectroscopy and using an electrochemical cell of Li|1 M $LiClO_4$ in EC:DEC = 1:1|$LiFePO_4$. $LiFePO_4$ nanoparticles with a geometric mean diameter of 58 nm were prepared at a rotating speed of 800 rpm and a ball-milling time of 12 h in an Ar atmosphere followed by heat treatment at 500 °C for 4 h in a N_2 + 3% H_2 atmosphere. The sample delivered first discharge capacities of 164 and 100 mAh g^{-1} at charge–discharge rates of 0.1 and 10 C in the test cells, respectively. The electrochemical properties of $LiFePO_4$ nanoparticles were strongly affected by the formation of Fe_2P, Fe_3P and α-Fe_2O_3 at higher charge–discharge rates.

1. Introduction

In recent years, the demand for the development of new cathode materials for high-performance lithium-ion batteries has increased continuously. $LiFePO_4$ is one of the most promising cathode materials for lithium-ion batteries owing to its relative lack of toxicity and the low cost and abundance of the raw materials. It also has a high lithium intercalation voltage of 3.4 V versus lithium metal and a high theoretical capacity of 170 mAh g^{-1} [1,2]. However, the performance of this material is limited by its poor electronic conductivity, which is a barrier preventing its large-scale application such as in hybrid electric vehicles (HEVs). Much effort has been developed to improving the electrochemical property of $LiFePO_4$ by reducing the particle size [3,4] or by coating $LiFePO_4$ particles with carbon [5–7] or a $LiFePO_4$/C composite [8–19]. As a result, the procedure of synthesis is becoming increasingly important, particularly when a reduced $LiFePO_4$ particle size and a carbon coating are required. Also, the formation of impurity phases such as α-Fe_2O_3 must be avoided to achieve full theoretical capacity [20]. To overcome the poor electronic conductivity, many synthesis routes have been developed, involving high-temperature solid-state reactions [1,2,9–12,21–25], the polyol process [3], the sol–gel process [8,13,21,26], hydrothermal synthesis [20,21,27–29], mechanical activation [6,18,30–36] and co-precipitation [37]. The majority of these synthesis routes require high sintering temperatures, long sintering times and several grinding steps. It is also difficult to precisely control the chemical composition of the as-prepared materials for the hydrothermal synthesis.

SP is a well-known continuous and single-step method for the preparation of fine homogeneous and multicomponent powders. Compared with particles obtained by conventional ceramic preparation methods, the particle size distribution is narrow and controllable from micrometer to submicrometer order, the purity of the products is high and the composition of the powders is easy to control. Even if the post-annealing of as-prepared powders by SP is required to obtain the desired materials, a shorter annealing time of the as-prepared powders can be expected in comparison with conventional ceramic preparation methods. In the contrary, several long sintering and regrinding procedures are needed to obtain the final product in the solid-state reaction method [25].

In our previous studies [38,39], a $LiFePO_4$/C composite and carbon-coated $LiFePO_4$ were prepared via SP and a combination of SP with dry ball-milling (DBM), respectively. However, the electrochemical performance of the prepared materials was not sufficient for large-scale application because the size of the $LiFePO_4$ particles was approximately 300 nm [39]. The reduction of particle size is a key factor for obtaining $LiFePO_4$ with a high rate capability. Thus,

* Corresponding author. Tel.: +81 3 5734 2155; fax: +81 3 5734 2155.
E-mail address: taniguchi.i.aa@m.titech.ac.jp (I. Taniguchi).

0378-7753/$ – see front matter © 2009 Elsevier B.V. All rights reserved.
doi:10.1016/j.jpowsour.2009.06.046

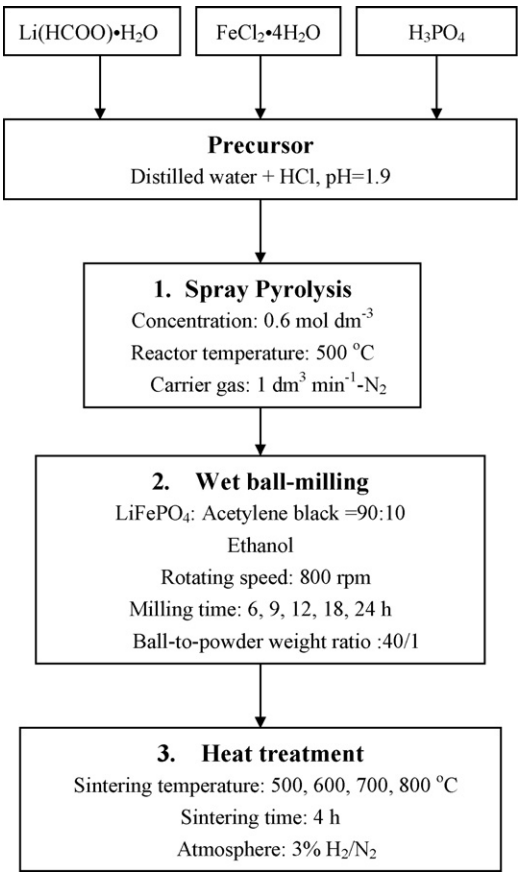

Fig. 1. Flow chart for the preparation of $LiFePO_4$ nanoparticles by the combination of SP with WBM followed by heat treatment.

we present a novel preparation technique for $LiFePO_4$ nanoparticles in this work.

2. Experimental

2.1. Preparation of $LiFePO_4$ nanoparticles

The precursor solution was prepared by dissolving the correct amount of $Li(HCOO)\cdot H_2O$, $FeCl_2\cdot 4H_2O$ and H_3PO_4 in distilled water in a stoichiometric ratio. The concentrations of Li^+, $Fe^{2+}$and PO_4^{3-} were all 0.2 mol dm^{-3}. The pH of the precursor solution was adjusted to 1.9 by adding HCl.

A schematic diagram of the SP setup was provided in our previous paper [40]. The precursor solution was atomized at a frequency of 1.7 MHz using an ultrasonic nebulizer. The sprayed droplets were transported to the reactor by N_2 gas. The flow rate of N_2 gas was fixed at 1 dm^3 min^{-1} and the reactor temperature was 500 °C. The as-prepared $LiFePO_4$ powder was milled by a planetary ball-mill (P-7, FRITSCH). To avoid $LiFePO_4$ particle growth during sintering [39], the as-prepared $LiFePO_4$ powder and acetylene black were mixed together at a weight ratio of 90:10 in the WBM process. Ethanol was used as a medium in the WBM process, which was carried out in an atmosphere of air or Ar gas. Zirconia balls and a 45-ml-volume zirconia vial were also used in the WBM process. The ball-to-powder weight ratio was 40:1 and the rotating speed was fixed at 800 rpm. The ball-milling time was also varied from 6 to 24 h. After the ball-milling, the samples were sintered at various temperatures from 500 to 800 °C for 4 h in a N_2 + 3% H_2 atmosphere in a tubular furnace. Fig. 1 shows the flow chart for the preparation of $LiFePO_4$ nanoparticles.

2.2. Sample characterization

The crystalline phase of the samples was identified by XRD analysis (Ultima IV with D/teX Ultra, Rigaku) with CoKα and CuKα radiation. The surface impurity of the samples was examined by Raman spectroscopy (NRS-2100, JASCO Co.) using the 514.5 nm line of an Ar ion laser. The particle size and morphology of the samples were examined by FE-SEM (S-800, Hitachi) and TEM (JEM-200CX, JEOL). The geometric mean diameter and geometric standard deviation were determined by randomly sampling approximately 500 particles from the TEM images. The specific surface area was also determined by the BET method (Flow Sorb II 2300, Shimadzu).

2.3. Fabrication of electrochemical cells and electrochemical characterization

Electrochemical characterization was performed by assembling a CR2032 coin cell for galvanostatic charge–discharge testing. The cell comprised a lithium metal electrode and a $LiFePO_4$/C electrode that were separated by a microporous polypropylene separator. 1 M $LiClO_4$ in EC:DEC = 1:1 (Tomiyama Pure Chemical Co. Ltd.) was used as the electrolyte. The cathode consisted of 78 wt.% $LiFePO_4$/C, 10 wt.% polyvinylidene fluoride (PVDF) as a binder and 12 wt.% acetylene black. Finally, the cathode contained 70 wt.% $LiFePO_4$, 20 wt.% acetylene black and 10 wt.% PVDF. These materials were dispersed in 1-methyl-2-pyrrolidinone (NMP), and the resultant slurry was then spread onto an aluminum foil using the doctor blade technique. The coated aluminum foil was dried for 4 h in an oven set at 110 °C and then pressed to achieve good adherence between the coated material and the aluminum foil. The cathode was formed by punching a circular disc from the foil and scraping it to standardize the area of the cathode (100 mm^2). The coin cell was assembled inside a glove box filled with high purity argon gas (99.9995% purity). The cell was cycled galvanostatically between 2.5 and 4.5 V using multichannel battery testers (HJ1010mSM8A, Hokuto Denko) at various charge–discharge rates ranging from 0.1 to 20 C at room temperature.

3. Results and discussion

3.1. Preparation and characterization of $LiFePO_4$ nanoparticles

Fig. 2 shows the XRD patterns of samples synthesized by SP at 500 °C and then ball-milled at 800 rpm for various times from 6 to 24 h followed by heat treatment at 500 °C for 4 h in a N_2 + 3% H_2 atmosphere. The JCPDS standard $LiFePO_4$ patterns are also shown in the figure. The diffraction peaks of all samples are identified as those of the orthorhombic structure with space group *Pnma* without any secondary phases such as Fe_2P and Fe_3P.

Fig. 3 shows the variation of the specific surface area of the $LiFePO_4$ samples with ball-milling time. The specific surface area considerably increases with ball-milling time up to 12 h. However, a further increase in ball-milling time results in the specific surface area gradually decreasing. This fact may indicate that both the milling and the agglomeration of $LiFePO_4$ and acetylene black powders simultaneously occurred during WBM. To clarify the effect of ball-milling time on the specific surface area, the powder morphology of the samples was also observed by SEM. Fig. 4 shows the result. For comparison, a SEM image of $LiFePO_4$ prepared at 500 °C by SP and then sintered at 500 °C for 4 h in a N_2 + 3% H_2 atmosphere is also shown in the figure (Fig. 4(C)). $LiFePO_4$ powders with a particle size of a few micrometers was synthesized by SP followed by heat treatment, while fine particles of $LiFePO_4$ were prepared by the present method with a ball-milling time of 12 h. However, significant particle aggregation occurs upon increasing the ball-milling time from 12 to 24 h.

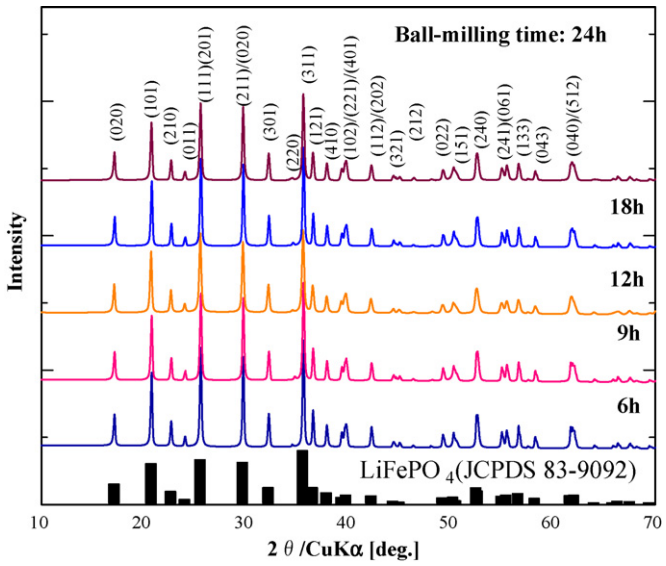

Fig. 2. XRD patterns of samples prepared by the combination of SP with WBM for various milling times in air followed by sintering at 500 °C.

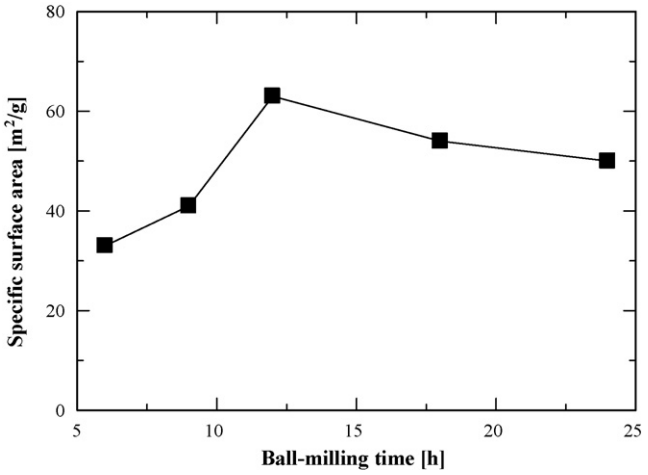

Fig. 3. Effect of ball-milling time on the specific surface area of $LiFePO_4$ samples prepared by the combination of SP with WBM for various milling times in air followed by sintering at 500 °C.

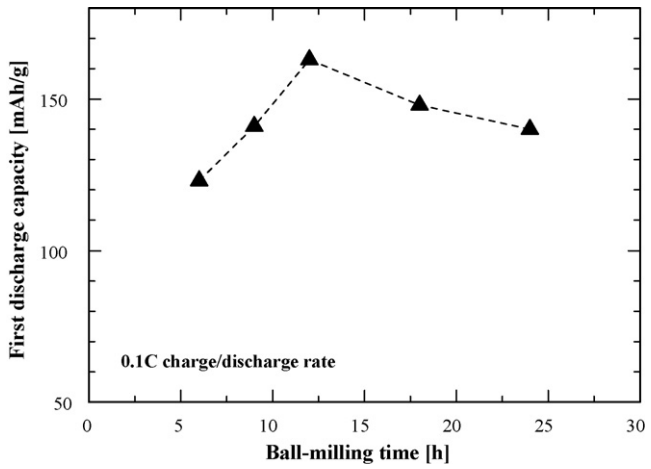

Fig. 5. Effect of ball-milling time on the first discharge capacity of $LiFePO_4$ samples prepared by SP at 500 °C with WBM for various ball-milling times in air followed by sintering at 500 °C.

Fig. 5 shows the effect of ball-milling time on the first discharge capacity of samples synthesized by SP at 500 °C and then milled at 800 rpm for various ball-milling times from 6 to 24 h followed by heat treatment at 500 °C for 4 h in a N_2 + 3% H_2 atmosphere. The charge–discharge rate is 0.1 C. The first discharge capacity increases with ball-milling time up to 12 h and has a maximum value (163 mAh g^{-1}) at 12 h. However, it then decreases with increasing ball-milling time. This may indicate that a $LiFePO_4$ sample with larger specific surface area has a larger discharge capacity, as shown in our previous work [38]. We were able to reconfirm that the electrochemical properties of the $LiFePO_4$ prepared by the present method are clearly affected by the specific surface area of the sample.

Fig. 6 shows the effect of sintering temperature on the specific surface area of $LiFePO_4$ samples. The samples were prepared at 500 °C by SP and then milled at 800 rpm for 12 h followed by heat treatment at various temperatures from 500 to 800 °C for 4 h in a N_2 + 3% H_2 atmosphere. The specific surface area slightly decreases with increasing sintering temperature due to the particle growth, which is clearly shown in Fig. 7. From the above-mentioned results, we can conclude that $LiFePO_4$ with the largest specific surface area can be prepared by the combination of SP at 500 °C with WBM at 800 rpm for 12 h followed by heat treatment at 500 °C for 4 h in a N_2 + 3% H_2 atmosphere.

To determine the particle size and distribution of samples, TEM was used. Fig. 8 shows TEM images of $LiFePO_4$ samples sintered at

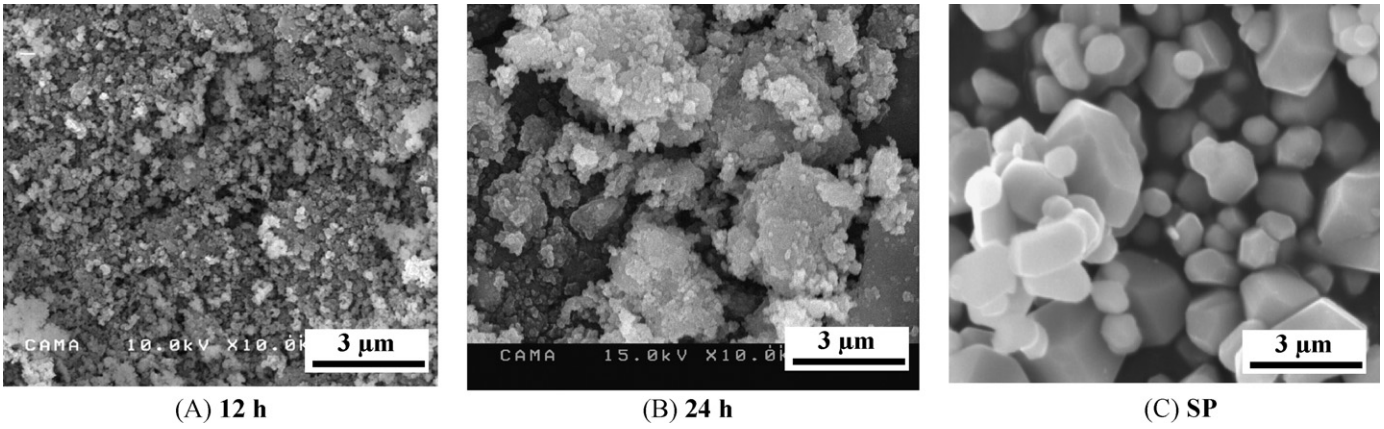

Fig. 4. SEM images of $LiFePO_4$ samples prepared by the combination of SP with WBM for ball-milling times of (A) 12 h and (B) 24 h in air followed by sintering at 500 °C (C).

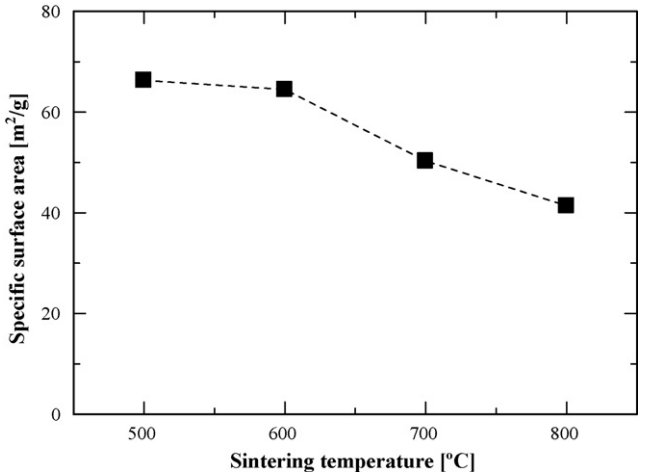

Fig. 6. Effect of sintering temperature on the specific surface area of $LiFePO_4$ samples prepared by the combination of SP at 500 °C with WBM for 12 h in air followed by sintering at various temperatures.

500 °C under low and high magnification. It is apparent that $LiFePO_4$ particles prepared by the combination of SP with WBM are less than 100 nm in size. The particle size distribution of $LiFePO_4$ is also shown in Fig. 9. The geometric mean diameter $d_{g,p}$ and standard deviation σ_g of the $LiFePO_4$ sample were 58 nm and 1.2, respectively. In our previous studies, we synthesized $LiFePO_4$ powders by SP [38] and a combination of SP with DBM [39], which were approximately 2 μm and 300 nm in size, respectively. However, $LiFePO_4$ nanoparticles with a geometric mean diameter of only 58 nm were successfully prepared by the present method.

The capacity loss of $LiFePO_4$ is well known to be caused by the utilization of large particle, whose small total surface area constrains the diffusion of lithium ions by decreasing the $LiFePO_4/FePO_4$ interface, as described by Padhi et al. [1]. They suggested that the electrochemical performance of the cathode can be improved by using small particles. The above-mentioned result clearly shows that the present method is effective for the preparation of $LiFePO_4$ nanoparticles.

3.2. Electrochemical performance of $LiFePO_4$ nanoparticles

The first charge–discharge profiles of the $LiFePO_4$ nanoparticles are shown in Fig. 10. The charge–discharge rate is 0.1 C. For comparison, those of $LiFePO_4$ produced by SP at 500 °C followed by heat treatment at 500 °C for 4 h in a N_2 + 3% H_2 atmosphere are also shown by dotted lines in the figure. The flat voltage plateau is at 3.4 V, corresponding to the Fe^{+2}/Fe^{+3} redox reaction. The $LiFePO_4$ nanoparticles have a discharge capacity of 163 mAh g^{-1}, which corresponds to 96% of the theoretical capacity of $LiFePO_4$ (170 mAh g^{-1}), while the $LiFePO_4$ sample prepared by SP with heat treatment delivers a discharge capacity of 82 mAh g^{-1}. Furthermore, the $LiFePO_4$ nanoparticles have a much smaller polarization loss and irreversible capacity.

The cycle performance of cells containing the $LiFePO_4$ nanoparticle samples was investigated for up to 100 cycles at different

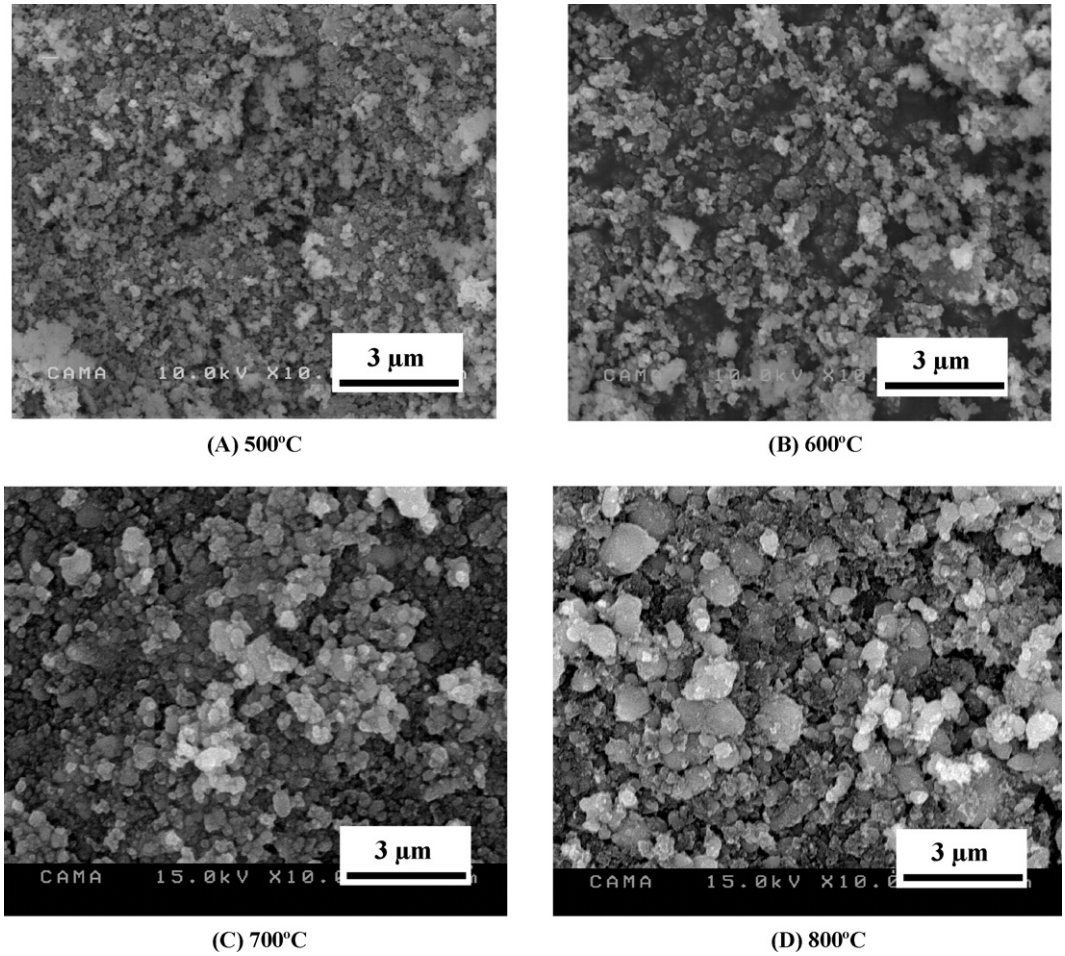

Fig. 7. SEM images of $LiFePO_4$ samples prepared by the combination of SP with WBM for 12 h in air followed by sintering at (A) 500 °C, (B) 600 °C, (C) 700 °C and (D) 800 °C.

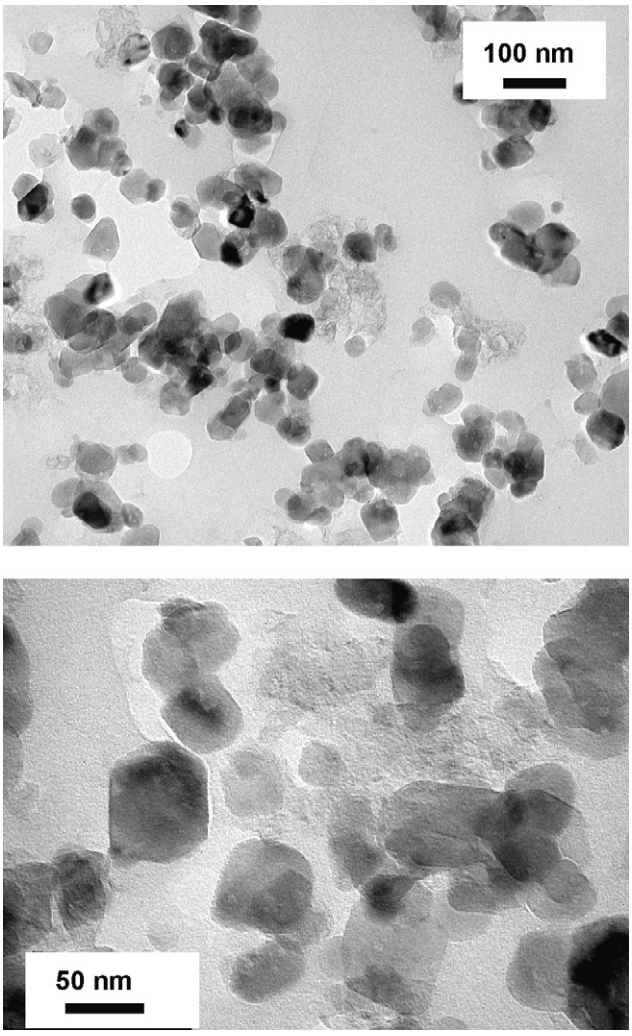

Fig. 8. TEM images of $LiFePO_4$ nanoparticles prepared by the combination of SP with WBM for 12 h in air followed by sintering at 500 °C.

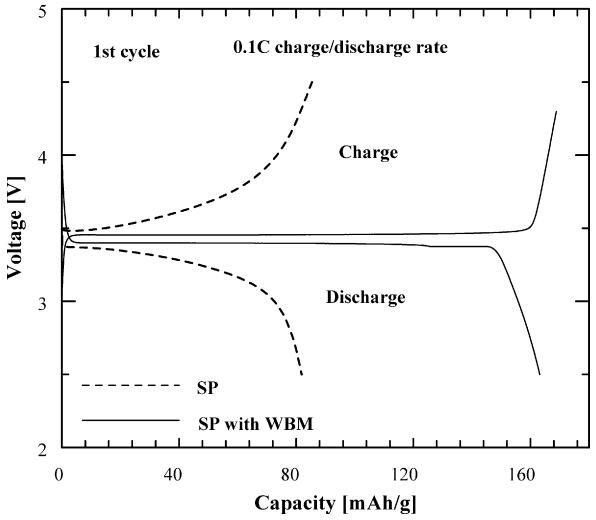

Fig. 10. First charge and discharge curves of $LiFePO_4$ nanoparticles prepared by the combination of SP with WBM for 12 h in air followed by sintering at 500 °C.

charge–discharge rates, and the results are given in Fig. 11. The $LiFePO_4$ nanoparticle cathode exhibits an excellent long-term cycling property. The cells retain 100% and 97% of their initial discharge capacities after 100 cycles at charge–discharge rates of 1 and 10 C, respectively.

Fig. 12 shows the rate capabilities of $LiFePO_4$ nanoparticles obtained by recording the first discharge capacities at charge–discharge rates from 0.1 to 20 C. For comparison, those of $LiFePO_4$ samples sintered at 600, 700 and 800 °C are also shown in the figure. The first discharge capacities of $LiFePO_4$ samples sintered at 500 °C at charge–discharge rates of 0.1, 1, 5, 10 and 20 C are 163, 154, 118, 97 and 15 mAh g^{-1}, respectively. The discharge capacity of the $LiFePO_4$ sample considerably decreases with increasing charge–discharge rates from 5 to 20 C. In contrast, the $LiFePO_4$ samples sintered at 600 °C exhibit first discharge capacities of 110 and 74 mAh g^{-1} even at charge–discharge rates of 10 and 20 C, respectively. The specific surface area of the $LiFePO_4$ samples sintered at 600, 700 and 800 °C are smaller than those of the samples sintered at 500 °C, as shown in Fig. 6. However, the discharge capacities of the $LiFePO_4$ sample sintered at 600 °C are larger than those of the $LiFePO_4$ sample sintered at 500 °C at charge–discharge rates from 5 to 20 C. To clarify the reason for this, the identification of small impurity phases by XRD analysis with CoKα radiation was

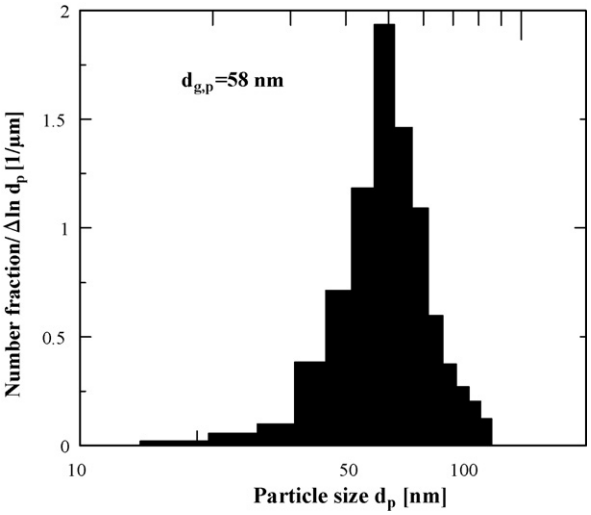

Fig. 9. Particle size distribution of $LiFePO_4$ nanoparticles prepared by the combination of SP with WBM for 12 h in air followed by sintering at 500 °C.

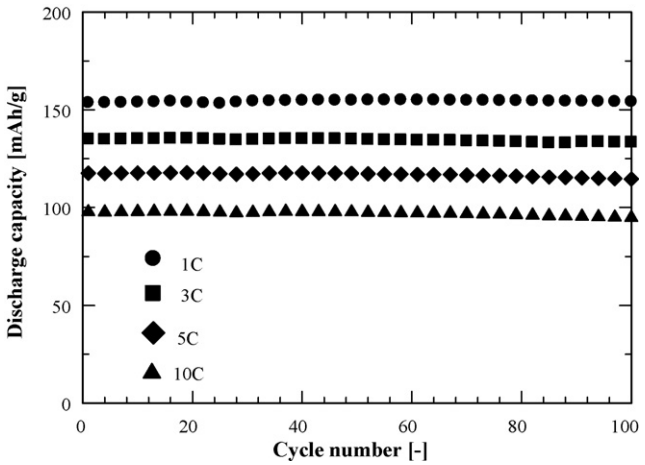

Fig. 11. Cycle performance of $LiFePO_4$ nanoparticles prepared by the combination of SP with WBM for 12 h in air followed by sintering at 500 °C.

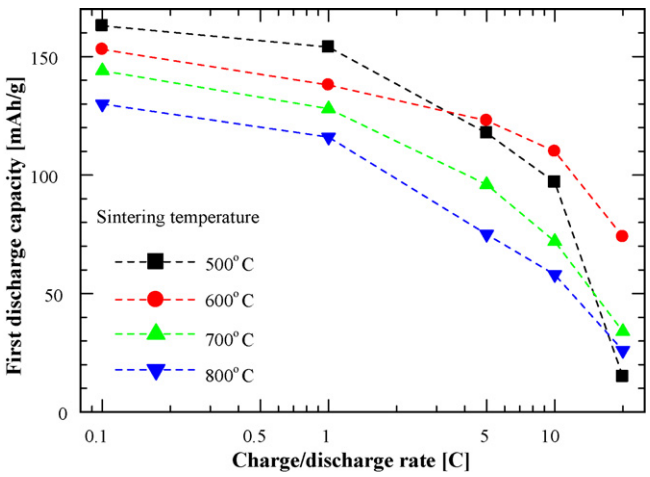

Fig. 12. Rate capabilities of $LiFePO_4$ samples prepared by the combination of SP at 500 °C with WBM for 12 h in air followed by sintering at various temperatures.

performed for $LiFePO_4$ samples sintered at different temperatures. Fig. 13 shows the XRD patterns of $LiFePO_4$ samples sintered at different temperatures. The $LiFePO_4$ sample sintered at 500 °C exhibits a pure $LiFePO_4$ olivine phase without any secondary phases. However, small impurity phases such as Fe_2P and Fe_3P were clearly identified in the $LiFePO_4$ samples sintered at 600, 700 and 800 °C. Furthermore, a small Fe peak is detected in the XRD patterns of $LiFePO_4$ samples sintered at 600 °C. The presence of these phases may be due to the fact that small amounts of Fe^{2+} and P^{5+} can be deoxidized to Fe, Fe_2P or Fe_3P by the acetylene black, which was mixed with $LiFePO_4$ to avoid $LiFePO_4$ particle growth during sintering, by providing a reductive environment. The formation of an Fe_2P or Fe_3P phase at high temperatures in a reductive environment has also been reported by Chung et al. [23], Xu et al. [17], Julien et al. [41], Mauger et al. [42] and Konarova and Taniguchi [38,39]. The formation of Fe_2P can improve the electrochemical conductivity of $LiFePO_4$, as recently reported by Kim et al. [32], while the discharge capacity may decrease with an increase in the amount of impurity phases due to a decrease in the amount of Fe^{2+} contributing to the charge–discharge process. For these reasons, the $LiFePO_4$ sample sintered at 600 °C delivers the largest discharge capacity at faster

Table 1
Effect of sintering temperature on the lattice parameters of $LiFePO_4$ nanopaticles.

Sintering temperature (°C)	Lattice parameters		
	a [Å]	*b* [Å]	*c* [Å]
500	6.003	10.323	4.695
600	6.007	10.330	4.691
700	6.007	10.330	4.691
800	6.008	10.331	4.692

charge–discharge rates ranging from 5 to 20 C.

The lattice parameters of the samples obtained from the XRD patterns based on the *Pnma* space group by Rietveld refinement are given in Table 1. The lattice parameters of the $LiFePO_4$ sample sintered at 500 °C showed good agreement with those reported in the literature [1]. However, the lattice parameters of $LiFePO_4$ samples sintered at 600, 700 and 800 °C are slightly different from the reported values. This reason is presently under study.

3.3. *Effect of α-Fe_2O_3 on the electrochemical properties of $LiFePO_4$ nanoparticles*

The surface structure was analyzed by Raman spectroscopy. Raman spectra of the $LiFePO_4$ sample sintered at 500 °C are illustrated in Fig. 14(a). Some peaks attributed to $LiFePO_4$ (441, 997 and 1067 cm^{-1}) [20,43] and carbon (1355 and 1590 cm^{-1}) [44–46] were detected in the Raman spectrum. Moreover, there are peaks at 213 and 277 cm^{-1}, which are attributed to a small amount of α-Fe_2O_3, which was not detected by XRD [20,38]. It was clarified that a small amount of α-Fe_2O_3 formed on the surface of the $LiFePO_4$ nanoparticles. As a result, this may indicate that a small amount of Fe^{2+} is oxidized to Fe^{3+} during the WBM process in air. Thus, WBM procedure was performed at 800 rpm for 12 h in Ar gas to prepare $LiFePO_4$ nanoparticles without α-Fe_2O_3, and the as-milled sample was then sintered at 500 °C for 4 h in a N_2 + 3% H_2 atmosphere. The Raman spectrum of this sample is shown in Fig. 14(b). It is clearly seen that there is no peak corresponding to α-Fe_2O_3.

The electrochemical characterization of pure $LiFePO_4$ nanoparticles was also performed at various charge–discharge rates. The sample was prepared by SP at 500 °C and then milled at 800 rpm for 12 h in Ar gas followed by sintering at 500 °C for 4 h in a N_2 + 3% H_2 atmosphere. The results are summarized in Table 2. The first

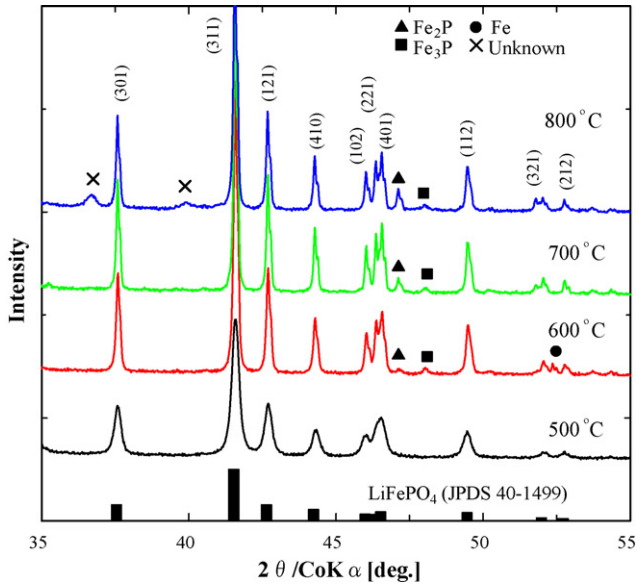

Fig. 13. XRD patterns (CoKα) of samples prepared by the combination of SP at 500 °C with WBM for 12 h in air followed by sintering at various temperatures.

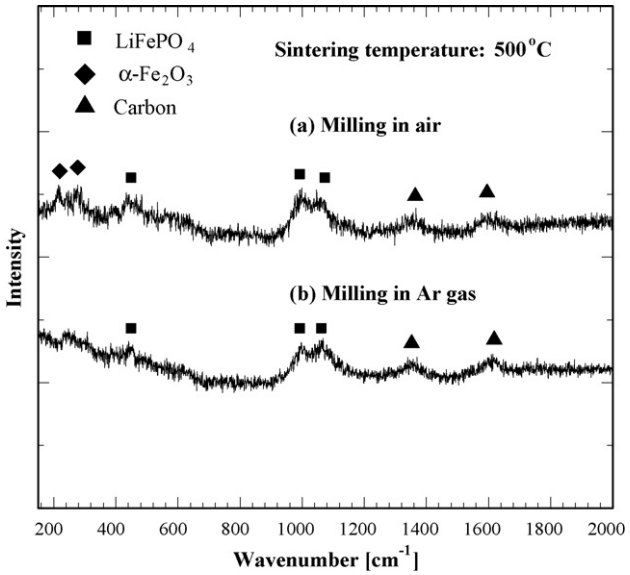

Fig. 14. Raman spectra of $LiFePO_4$ nanoparticles prepared by the combination of SP at 500 °C with WBM for 12 h in (a) air and (b) Ar gas followed by sintering at 500 °C.

Table 2
Effect of α-Fe_2O_3 on the electrochemical properties of $LiFePO_4$ nanoparticles.

Ball-milling condition (atmosphere)	First discharge capacity [mAh g^{-1}]				
	0.1 C	1 C	5 C	10 C	20 C
Air	163	153	114	81	15
Ar gas	164	155	118	100	41

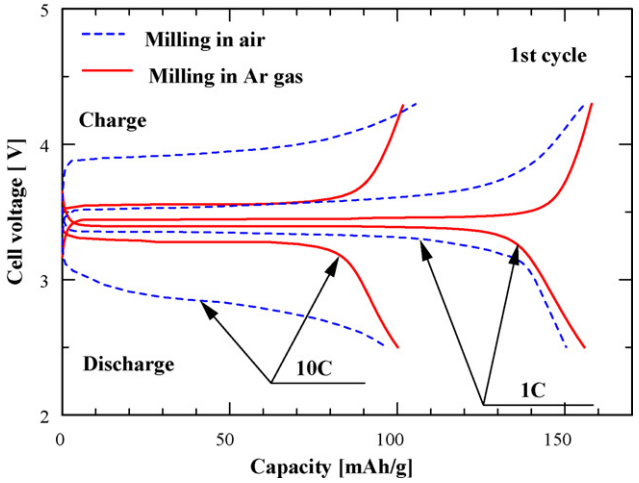

Fig. 15. Charge and discharge profiles of $LiFePO_4$ nanoparticles prepared by the combination of SP at 500 °C with WBM for 12 h in (a) air and (b) Ar gas followed by sintering at 500 °C.

discharge capacities of $LiFePO_4$ milled in Ar gas are larger than those of $LiFePO_4$ milled in air at charge–discharge rates from 10 to 20 C, while there is no significant difference between the $LiFePO_4$ samples milled in Ar gas and air at low charge–discharge rates. Fig. 15 shows the first charge–discharge curves of the samples at charge–discharge rates of 1 and 10 C. For the purpose of comparison, those of the $LiFePO_4$ sample milled in air are represented by dotted lines in the figure. The sample milled in Ar gas exhibits a high voltage difference between the charge and discharge plateaus, particularly at a high charge–discharge rate. This may indicate that the polarization loss considerably increases at a high charge–discharge rate (10 C) owing to the formation of α-Fe_2O_3 on the surface of $LiFePO_4$ nanoparticles. It can be concluded that the formation of α-Fe_2O_3 on the surface of $LiFePO_4$ nanoparticles significantly affects the kinetics of $LiFePO_4$ during the electrochemical process.

4. Conclusions

$LiFePO_4$ nanoparticles were successfully prepared by the combination of SP with WBM at 800 rpm for 12 h in Ar gas followed by heat treatment at 500 °C for 4 h in a N_2 + 3% H_2 atmosphere. XRD patterns of $LiFePO_4$ nanoparticles were assigned to an ordered olivine structure indexed by orthorhombic *Pnma*. TEM observation demonstrated that $LiFePO_4$ particles with a geometric mean diameter of 58 nm were obtained by the present method. The $LiFePO_4$ nanoparticles exhibited first-discharge capacities of 164 mAh g^{-1} at 0.1 °C and 100 mAh g^{-1} at 10 °C. They also retained 100% and 97% of their initial discharge capacities after 100 cycles at charge–discharge rates of 1 and 10 C, respectively. The electrochemical properties of $LiFePO_4$ nanoparticles were strongly affected by the formation of α-Fe_2O_3, Fe_2P and Fe_3P at high charge–discharge rates.

Acknowledgments

This research was partially supported by Development of an Electric Energy Storage System for Grid-connection with New Energy Resources in New Energy and Industrial Technology Development Organization. The authors are grateful to the staff members (Mr. A. Genseki and Mr. J. Koki) of the Center for Advanced Materials Analysis (Tokyo Institute of Technology, Japan) for help in the TEM observation of as-prepared powders. Moreover, the authors gratefully acknowledge the assistance of Ms. M. Saigou (Rigaku Co. Ltd.) in carrying out XRD analysis and Rietveld refinement.

References

[1] K. Padhi, K.S. Nanjundaswamy, J.B. Goodenough, J. Electrochem. Soc. 144 (1997) 1188.
[2] A.K. Padhi, K.S. Nanjundaswamy, C. Masquelier, S. Okada, J.B. Goodenough, J. Electrochem. Soc. 144 (1997) 1609.
[3] D.-H. Kim, J. Kim, Electrochem. Solid-State Lett. 9 (2006) A439.
[4] C. Delacourt, P. Poizot, S. Levasseur, C. Masquelier, Electrochem. Solid-State Lett. 9 (2006) A352.
[5] K. Zaghib, N. Ravet, M. Gauthier, F. Gendron, A. Mauger, J.B. Goodenough, C.M. Julien, J. Power Sources 163 (2006) 560.
[6] H.C. Shin, W.I. Cho, H. Jang, Electrochim. Acta 52 (2006) 1472.
[7] I. Belharouak, C. Johnson, K. Amine, Electrochem. Commun. 7 (2005) 983.
[8] H. Huang, S.-C. Yin, L.F. Nazar, Electrochem. Solid-State Lett. 4 (2001) A170.
[9] Z. Chen, J.R. Dahn, J. Electrochem. Soc. 149 (2002) A1184.
[10] E.M. Bauer, C. Bellitto, M. Pasquali, P.P. Prosini, G. Righini, Electrochem. Solid-State Lett. 7 (2004) A85.
[11] P.P. Prosini, D. Zane, M. Pasquali, Electrochim. Acta 46 (2001) 3517.
[12] G.T.-K. Fey, T.-L. Lu, J. Power Sources 178 (2008) 807.
[13] C.R. Sides, F. Croce, V.Y. Young, C.R. Martin, B. Scrosati, Electrochem. Solid-State Lett. 8 (2005) A484.
[14] R. Dominko, M. Gaberscek, J. Drofenik, M. Bele, S. Pejovnik, J. Jamnik, J. Power Sources 119–121 (2003) 770.
[15] S.L. Bewlay, K. Konstantinov, G.X. Wang, S.X. Dou, H.K. Liu, Mater. Lett. 58 (2004) 1788.
[16] M.-R. Yang, T.-H. Teng, S.-H. Wu, J. Power Sources 159 (2006) 307.
[17] Y. Xu, Y. Lu, L. Yan, Z. Yang, R. Yang, J. Power Sources 160 (2006) 570.
[18] S. Franger, C. Benoit, C. Bourbon, F.L. Cras, J. Phys. Chem. Solids 67 (2006) 1338.
[19] V. Palomares, A. Goñi, I.G. de Muro, I. de Meatza, M. Bengoechea, O. Miguel, T. Rojo, J. Power Sources 171 (2007) 879.
[20] K. Dokko, K. Shiraishi, K. Kanamura, J. Electrochem. Soc. 152 (2005) A2199.
[21] M. Koltypin, D. Aurbach, L. Nazar, B. Ellis, J. Power Sources 174 (2007) 1241.
[22] D. Wang, H. Li, S. Shi, X. Huang, L. Chen, Electrochem. Acta 50 (2005) 2955.
[23] S.Y. Chung, J.T. Bloking, Y.M. Chiang, Nature Mater. 1 (2002) 123.
[24] P.S. Herle, B. Ellis, N. Coombs, L.F. Nazar, Nature Mater. 3 (2004) 147.
[25] A. Yamada, S.C. Chung, K. Hinokuma, J. Electrochem. Soc. 148 (2001) A224.
[26] D. Choi, P.N. Kumta, J. Power Sources 163 (2007) 1064.
[27] D.Y.W. Yu, C. Fietzek, W. Weydanz, K. Donoue, T. Inoue, H. Kurokawa, S. Fujitani, J. Electrochem. Soc. 154 (2007) A253.
[28] X. Ou, G. Liang, L. Wang, S. Xu, X. Zhao, J. Power Sources 184 (2008) 538.
[29] G. Meligrana, C. Gerbaldi, A. Tuel, S. Bodoardo, N. Penazzi, J. Power Sources 160 (2006) 516.
[30] J.-K. Kim, G. Cheruvally, J.-W. Choi, J.-U. Kim, J.-H. Ahn, G.-B. Cho, K.-W. Kim, H.-J. Ahn, J. Power Sources 166 (2007) 211.
[31] J.-K. Kim, J.-W. Choi, G. Cheruvally, J.-U. Kim, J.-H. Ahn, G.-B. Cho, K.-W. Kim, H.-J. Ahn, Mater. Lett. 61 (2007) 3822.
[32] C.W. Kim, J.S. Park, K.S. Lee, J. Power Sources 163 (2006) 144.
[33] K. Wang, R. Cai, T. Yuan, X. Yu, R. Ran, Z. Shao, Process investigation, electrochemical characterization and optimization of $LiFePO_4$/C composite from mechanical activation using sucrose as carbon source, Electrochim. Acta 54 (2009) 2861.
[34] G.T.-K. Fey, Y.G. Chen, H.-M. Kao, Electrochemical properties of $LiFePO_4$ prepared via ball-milling, J. Power Sources 189 (2009) 169.
[35] J.-K. Kim, G. Cheruvally, J.-H. Ahn, G.-C. Hwang, J.-B. Choi, J. Phys. Chem. Solids 69 (2008) 2371.
[36] H.-C. Kang, D.-K. Jun, B. Jin, E.M. Jin, K.-H. Park, H.-B. Gu, K.-W. Kim, J. Power Sources 179 (2008) 340.
[37] G. Arnold, J. Garche, R. Hemmer, S. Strobele, C. Vogler, M. Wohlfahrt-Mehrens, J. Power Sources 119–121 (2003) 247.
[38] M. Konarova, I. Taniguchi, Mater. Res. Bull. 43 (2008) 3305.
[39] M. Konarova, I. Taniguchi, Powder Technol. 191 (2009) 111.
[40] I. Taniguchi, C.K. Lim, D. Song, M. Wakihara, Solid State Ionics 146 (2002) 239.
[41] C.M. Julien, A. Mauger, A. Ait-Salah, M. Massot, F.K. Gendron, Ionics 13 (2007) 395.
[42] A. Mauger, A. Ait-Salah, M. Massot, F. Gendron, K. Zaghib, C.M. Julien, ECS Trans. 3–36 (2007) 57.
[43] C.M. Burba, R. Frech, J. Electrochem. Soc. 151 (2004) A1032.
[44] S.-W. Song, R.P. Reade, R. Kostecki, K.A. Striebel, J. Electrochem. Soc. 153 (2006) A12.
[45] M.M. Doeff, Y. Hu, F. McLarnon, R. Kostecki, Electrochem. Solid-State Lett. 6 (2003) A207.
[46] Y. Hu, M.M. Doeff, R. Kostecki, R. Fiñones, J. Electrochem. Soc. 151 (2004) A1279.